01 Feb 2016

Calculated Vibrational States of Ozone up to Dissociation

Steve Alexandre Ndengué

Richard Dawes
Missouri University of Science and Technology, dawesr@mst.edu

Xiaogang Wang

Tucker Carrington Jr.

et. al. For a complete list of authors, see https://scholarsmine.mst.edu/chem_facwork/2500

Recommended Citation

S. A. Ndengué et al., "Calculated Vibrational States of Ozone up to Dissociation," *Journal of Chemical Physics*, vol. 144, no. 7, American Institute of Physics (AIP), Feb 2016.
The definitive version is available at https://doi.org/10.1063/1.4941559

Calculated vibrational states of ozone up to dissociation

Steve Ndengué,[1] Richard Dawes,[1,a)] Xiao-Gang Wang,[2,a)] Tucker Carrington, Jr.,[2,a)] Zhigang Sun,[3] and Hua Guo[4]
[1]*Department of Chemistry, Missouri University of Science and Technology, Rolla, Missouri 65409, USA*
[2]*Chemistry Department, Queen's University, Kingston, Ontario K7L 3N6, Canada*
[3]*State Key Laboratory of Molecular Reaction Dynamics and Center for Theoretical and Computational Chemistry, Dalian Institute of Chemical Physics, Chinese Academy of Sciences, Dalian 116023, China and Center for Advanced Chemical Physics and 2011 Frontier Center for Quantum Science and Technology, University of Science and Technology of China, 96 Jinzhai Road, Hefei 230026, China*
[4]*Department of Chemistry and Chemical Biology, University of New Mexico, Albuquerque, New Mexico 87131, USA*

(Received 21 December 2015; accepted 22 January 2016; published online 17 February 2016)

A new accurate global potential energy surface for the ground electronic state of ozone [R. Dawes *et al.*, J. Chem. Phys. **139**, 201103 (2013)] was published fairly recently. The topography near dissociation differs significantly from previous surfaces, without spurious submerged reefs and corresponding van der Waals wells. This has enabled significantly improved descriptions of scattering processes, capturing the negative temperature dependence and large kinetic isotope effects in exchange reaction rates. The exchange reactivity was found to depend on the character of near-threshold resonances and their overlap with reactant and product wavefunctions, which in turn are sensitive to the potential. Here we present global "three-well" calculations of all bound vibrational states of three isotopic combinations of ozone ($^{48}O_3$, $^{16}O_2{}^{18}O$, $^{16}O_2{}^{17}O$) for $J = 0$ and $J = 1$ with a focus on the character and density of highly excited states and discuss their impact on the ozone isotopic anomaly. The calculations were done using a parallel symmetry-adapted Lanczos method with the RV3 code. Some comparisons were made with results obtained with the improved relaxation method implemented in the Heidelberg multi-configuration time-dependent Hartree code. © *2016 AIP Publishing LLC.* [http://dx.doi.org/10.1063/1.4941559]

I. INTRODUCTION

Ozone is an important species in the atmosphere. Besides its crucial role of filtering harmful solar UV radiation, it participates in secondary chemistry of numerous species such as CO_2,[1,2] SO_2, NO_2, N_2O,[3] ClO_2, and ozonolysis of alkenes leading to Criegee intermediates.[4–8] Ozone is continually regenerated in the atmosphere according to the Chapman cycle,[9]

$$O_2 + h\nu \rightarrow O + O, \tag{1}$$

$$O + O + M \rightarrow O_2 + M, \tag{2}$$

$$O_2 + O + M \rightarrow O_3^* + M \rightarrow O_3 + M^*, \tag{3a}$$

$${}^yO^zO + {}^xO \rightarrow O_3^* \rightarrow {}^xO^zO + {}^yO \text{ or } {}^yO^xO + {}^zO, \tag{3b}$$

$$O_3 + h\nu \rightarrow O_2 + O, \tag{4}$$

$$O_3 + O \rightarrow 2O_2, \tag{5}$$

with additional destruction by chemical reactions. Step (3b) represents the isotope exchange reactions that may occur in the absence of stabilizing collisions leading to formation (step (3a)). Since the early 1980s, Thiemens and Heidenreich[10] and Mauersberger[11] have reported significant discrepancies between expected and observed ozone isotopic ratios in the troposphere, the stratosphere, and the laboratory. This phenomenon, known as the ozone isotopic anomaly or the mass independent fractionation (MIF) of ozone, tends to favor the formation of heavy and *asymmetric* isotopologues over the lighter and symmetric ones.[12,13] There is evidence indicating that this is partly because formation (step (3a)) is in competition with the exchange processes (step (3b)) which are governed by near-threshold reactive resonances and are most efficient for wavefunctions of *symmetric* isotopologues that overlap with reactant and product states.[14] After more than three decades of investigation, a view of the mechanisms involved in the non-statistical dynamics causing the ozone isotopic anomaly is emerging. At the present time, the mass dependent fractionation (MDF) contribution of the photodissociation processes is known reasonably accurately[15–18] and it appears that the MIF signature comes primarily from the ozone formation process. It is clear that a correct description of the isotopic anomaly through the calculation of formation/recombination rates requires an accurate description of the ground state potential energy surface (PES): illustrative examples are the recent calculations of $O + O_2$ exchange reaction rates by two and three-dimensional quantum statistical models[19,20] and the rigorous quantum scattering calculations[21,22] that show for the first time the negative temperature dependence and large kinetic isotope effect seen in experiments.

In the past 15 years, several calculations of the ground state PES of ozone have been reported.[20,23–28] The PES

a)Authors to whom correspondence should be addressed. Electronic addresses: dawesr@mst.edu; xgwang.dalian@gmail.com; and Tucker.Carrington@queensu.ca

by Siebert *et al.* (SSB)[23,24] later modified by Babikov[28] (mSSB) has been used extensively in theoretical studies of spectroscopy (bound states and resonances) and dynamics. The low-lying vibrational levels on the mSSB PES are remarkably accurate. The main deficiency of the mSSB PES is a submerged reef along the $O_2 + O \rightarrow O_3$ minimum energy pathways of the PES and corresponding shallow van der Waals (vdW) wells. The reef feature dramatically affects (reduces) low temperature exchange rate coefficients and causes their positive temperature dependence contrary to experiment.

In 2003, the highest lying bound states of the mSSB PES were reported by Grebenshchikov *et al.*[27] and also by Babikov.[29] Despite using the same PES, due to some differences in approach and the difficulty of converging all of the hundreds of bound states, significantly different results were obtained, especially for the highest lying states. This was clarified in 2004 through the work of Lee and Light.[30] For the isotopologues with three identical nuclei ($^{48}O_3$, $^{51}O_3$, $^{54}O_3$), hyperspherical coordinates have the important advantage that they treat the three equivalent isomers (see Figure 1) on an equal footing. Previous studies have labelled the states by the irreducible representations A_1, A_2, and E of the C_{3V}(M) group.[29,30] We will discuss symmetry in more detail later. In practice, a large basis is required to achieve convergence when using hyperspherical coordinates to describe the high-lying states of ozone.[31] The requirement for a large basis (especially for the θ and φ coordinates) makes it difficult to combine hyperspherical coordinates with direct diagonalization even today. As noted by Lee and Light, if sufficiently large coordinate ranges and numbers of basis functions are used, then the results should be independent of the coordinate system.[30] Indeed, by using a large basis of $\sim 1.9 \times 10^6$ discrete variable representation (DVR) functions and the Lanczos method to obtain eigenvalues, Lee and Light produced results in hyperspherical coordinates that closely match those of Grebenshchikov *et al.* who also used a large DVR grid, but Jacobi coordinates.[27]

On the mSSB PES, the spurious vdW wells localize bound states which are denser, close to the dissociation threshold, than the states with amplitude in the main wells. Except for few mixed eigenstates, they are generally decoupled from the main well states; that is, they follow different vibrational progressions.[27] Since the reef persists in some very high-level electronic structure calculations (e.g., MRCI(Q)/CBS),[25] efforts were made to reconcile the rates of

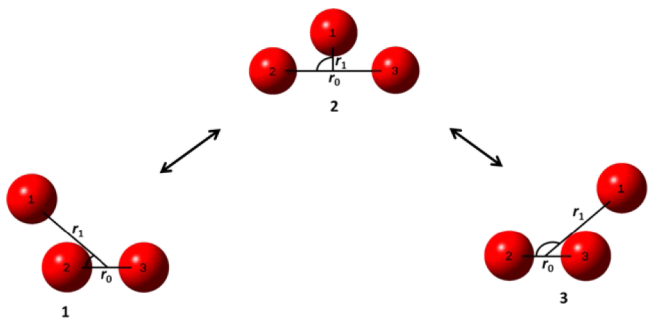

FIG. 1. Illustration of the three equivalent wells for O_3, described in Jacobi coordinates (see text).

exchange and formation with the presence of a reef and the corresponding vdW states. Babikov proposed helium nanodroplet experiments with which one might observe such states[29] and also explored the possibility of collisional transfer of population between vdW states and those localized in the main wells.[32] The dynamics calculated for this mechanism are not consistent with experimental rates of exchange and formation, and no observations of vdW states have been reported.

We recently reported a new global PES[20] (referred to as DJLLG) for the ground electronic state of ozone where the reef, a signature of the mSSB PES, disappears and the energy decreases monotonically along the minimum energy path to formation. The reef is caused mainly by an avoided crossing with an excited state. The electronic state character in the wells is primarily $O(^1D) + O_2(^1\Delta_g)$,[33,34] and dissociation forms those fragments diabatically. However, adiabatically dissociation connects to $O(^3P) + O_2(^3\Sigma_g^-)$ since the states switch character. This has implications for the symmetry of allowed rovibrational states that will be discussed later. By including numerous excited states in the calculation using a dynamic weighting procedure, the switch in state character occurs more smoothly without the reef barrier. The sensitivity of the reef to aspects of the electronic structure calculations has been described previously in Refs. 19 and 20 but a few details are given in Sec. II. The DJLLG PES possesses five qualities that make it suitable for dynamics calculations: (1) excellent equilibrium structural parameters, (2) good agreement with experimental vibrational levels, (3) accurate dissociation energy, (4) a transition region with accurate topography including a spin-orbit correction, and (5) three equivalent wells smoothly connected and representing full permutation symmetry. Previously computed PESs such as mSSB met some of these criteria but are generally lacking the accurate topography in the transition region and the accurate dissociation energy. Levels computed with a one-well method on the recent spectroscopic PES by Tyuterev *et al.*[26] match the experimental band origins very closely up to 7900 cm^{-1} (about 664 cm^{-1} below the best current estimate of the dissociation limit, $D_0 = 8563.5 \pm 3.5$ cm^{-1}).[35] Experimental assignments have not yet been made closer to dissociation (beyond $\sim$7900 cm^{-1}) but are being actively pursued.[36,37] Notably, a version of the Tyuterev PES that includes a *Dawes correction* to remove the reef feature produces improved agreement with the highest assigned levels just below 7900 cm^{-1}.[26] The confining effect of the spurious reef pushes up the levels and is felt as far as 800 cm^{-1} below dissociation. The Tyuterev PES slightly underestimates the dissociation energy and does not yet account for spin-orbit effects that shape the topography and further lower the dissociation energy. Nevertheless, it continues to guide the experimental team in the challenge of measuring and assigning states ever closer to dissociation.[36,37]

As mentioned above, the DJLLG PES has been used in several scattering studies and yields significantly improved agreement with observed exchange rates, capturing their negative temperature dependence and large kinetic isotope effect.[14,21,38,39] Given the importance of near-threshold resonances, just above dissociation, noted in those studies,[14,38] here we focus on the density and character of

the highest-lying bound states just below. These states are relevant to understanding the character of the most important resonances that overlap with reactant and product states in the exchange processes as well as characterizing the progressions of uppermost states that are populated through the collisional stabilization of resonances in the formation process. In this publication, we report all of the bound vibrational states of three isotopic combinations of ozone ($^{48}O_3$, $^{16}O_2{}^{18}O$, $^{16}O_2{}^{17}O$) for $J = 0$ and $J = 1$, simultaneously taking into account the three wells, computed with symmetry adapted rovibrational basis functions in Jacobi coordinates using the Lanczos algorithm.

Future studies of the resonances above the dissociation threshold are being considered, including investigations of collisional stabilization of the resonances and high-lying bound states through inelastic collisions with a third body such as argon. The multi-configuration time-dependent Hartree (MCTDH) method[40,41] has proven to be an accurate and efficient approach to compute both resonances and state-to-state inelastic cross sections.[42,43] To set the stage for such further studies, we also tested the performance of the MCTDH package to compute some of the bound states. Ideally, given a close correspondence between the MCTDH and Lanczos results, the wavefunctions produced by Lanczos and saved on a grid can be used as initial eigenstates for inelastic third-body scattering calculations with MCTDH.

This paper is organized as follows: in Section II, we briefly describe the underlying electronic structure calculations of the DJLLG PES, and detail the theoretical methods for the calculation of vibrational states. In Section III, we discuss our results and conclude in Section IV with an outlook for the future. Complete tables of all the computed levels are available as the supplementary material.[44]

II. THEORETICAL METHODS

A. Electronic structure

The electronic structure details of the DJLLG PES have been reported previously[19,20] so only a brief summary is given here. The global PES was fit using explicitly correlated MRCI-F12/VQZ-F12 data[45,46] based on a 20-state dynamically weighted, full-valence CASSCF reference, computed using the MOLPRO[47] quantum chemistry package. An automated PES generation method[48–52] was used to fit the surface out to r_1(O–OO) = 10 bohrs in Jacobi coordinates including 2663 symmetry unique *ab initio* data, with symmetry equivalent points generated by permutation. r_0 is the internuclear distance of the O_2 fragment, while r_1 is the distance from the center-of-mass of O_2 to the third O-atom (see Figure 1). No bias was used for the point selection, so the four wells (including the high-energy ring minimum) and the asymptotic region were treated equally. Between 8 and 10 bohrs the PES is switched to the long-range interaction model of O_2 + O by Lepers *et al.*,[53] which was extended to account for the r_0-dependence of the O_2 + O interaction.[54] The r_0-dependence of the asymptotic O_2 fragment itself is obtained by switching simultaneously to the accurate potential energy curve (PEC) of Ruedenberg *et al.*[55] A spin-orbit (SO) coupling correction, also present in the long-range model of Lepers *et al.*, was added to the PES. The geometric parameters of the three C_{2v} global minima are r_e = 2.4031 bohrs and θ_e = 116.84°, while the D_{3h} ring minimum is found at an optimized structure of r_e = 2.7153 with an energy of 10 755 cm^{-1} (1481 cm^{-1}) above the dissociation energy (D_e). The value of D_e for the DJLLG PES is 9355 cm^{-1} which reduces to 9275 cm^{-1} including the spin-orbit correction (slightly above the experimental value of 9219 ± 10.0 cm^{-1}).[20,26]

B. Lanczos calculations

The rovibrational basis functions used for the symmetry adapted Lanczos calculations are products of stretch basis functions $g^{(0)}_{k_{r_0}}(r_0)g^{(1)}_{k_{r_1}}(r_1)$ and bend-rotation functions. r_0 and r_1 are Jacobi vectors. A shared-K FBR (SKF) basis is chosen for the bend-rotation basis.[56] It is a non-direct product of an associated Legendre function and a symmetric-top function

$$\langle \theta_1;\alpha,\beta,\gamma|l_1;JKM\rangle = \Theta^{m_1}_{l_1}(\theta_1)\langle\alpha,\beta,\gamma\,|JKM\rangle\,, \qquad (6)$$

where $\Theta^{m_1}_{l_1}(\theta_1)$ is a normalized associated Legendre function with the $(-1)^{m_1}$ Condon-Shortley phase factor, $\langle\alpha,\beta,\gamma|JKM\rangle$ is a symmetric-top function with (α,β,γ) being the Euler angles and $m_1 \equiv K$. With this choice of m_1, all matrix elements of the Kinetic Energy Operator (KEO) are finite and simple. In the following, M is dropped since it is a good quantum number. Knowing that the inversion operator E^* affects the angles (it has no effect on r_i)

$$E^* f(\theta_1;\alpha,\beta,\gamma) = f(\theta_1,\pi+\alpha,\pi-\beta,\pi-\gamma), \qquad (7)$$

where f is some arbitrary function, we determine that $E^*|l_1;JK\rangle = (-1)^J|l_1;J\bar{K}\rangle$. The parity adapted basis functions are therefore

$$u^{JP}_{l_1;K} = N_K\frac{1}{\sqrt{2}}\left[|l_1;JK\rangle + (-1)^{J+P}|l_1;J\bar{K}\rangle\right] \qquad (8)$$

with $N_K = (1+\delta_{K,0})^{-1/2}$ and $\bar{K} = -K$, where $K \geq 0$ for $(-1)^{J+P} = 1$ and $K \geq 1$ for $(-1)^{J+P} = -1$. $P = 0$ and 1 correspond to even and odd parity, respectively. The molecule-fixed axes are chosen so that the z-axis is along r_0 and the x-axis is $r_0 \times r_1 \times r_0$ which is in the plane of the molecule. The KEO is well known.[56]

The permutation operator, denoted by σ_{ex}, permutes the two oxygen atoms connected by r_0 and flips the vector. It also affects the molecule-fixed frame such that the y- and z-axes are flipped and the x-axis is unchanged. For the parity-adapted rotational functions R^P_{JK} and parity-adapted rovibrational functions $u^{JP}_{l_1;K}$, the permutation operator acts as follows:

$$\sigma_{ex}u^{JP}_{l_1;JK} = (-1)^{l_1+P}u^{JP}_{l_1;JK}. \qquad (9)$$

Because we use Jacobi coordinates, we work with G4 = {E,E*} × {E, σ_{ex}}, a subgroup of the full PI group G12, or MS group D_{3h}(M).[57] The G4 group has irreducible representations (irreps) A^+, B^+, A^-, B^-. The basis functions are easily symmetry-adapted for each irrep by restricting the evenness and oddness of l_1. The correlation between G_4 irreps and D_{3h}(M) irreps is given in Table I. We define the irreps of G_4 group so that a B irrep is anti-symmetric under (23) = σ_{ex}

TABLE I. Correlation between the irreps of full PI group G_{12} or $D_{3h}(M)$ and subgroup G_4 or $C_{2v}(M)$ for $^{48}O_3$ calculations, derived from Tables A-5 and A-10 of Ref. 57.

$D_{3h}(M)$	E	(23)	E*	(23)*	G_4	$C_{2v}(M)$
A_1'	1	1	1	1	A^+	A_1
A_1''	1	1	−1	−1	A^-	A_2
A_2'	1	−1	1	−1	B^+	B_2
A_2''	1	−1	−1	1	B^-	B_1
E′	2	0	2	0	$A^+ \oplus B^+$	$A_1 \oplus B_2$
E″	2	0	−2	0	$A^- \oplus B^-$	$A_2 \oplus B_1$

and a "−" irrep is anti-symmetric under E*. In this paper, we choose to use G_4 irreps; the corresponding $D_{3h}(M)$ irreps can be recovered if needed.

The G_4 group is isomorphic to the C_{2v} point group which is the symmetry group of O_3 localized in one well. Irreps of C_{2v} have been used to discuss rovibrational spectra of O_3.[26,58] Note that the B_1 and B_2 irreps of Flaud and Bacis[58] are swapped from the convention of Bunker and Jensen,[57] which we follow.

Lee and Light used a subgroup $C_{3v}(M)$ to label vibrational levels of O_3, but this only applies to the vibrational states and is not sufficient for our $J > 0$ calculations. Since all the vibrational states are of even parity, the correlation between the irreps of $C_{3v}(M)$ and G_4 group is such that A_1, A_2, and E of $C_{3v}(M)$ correspond to A^+, B^+, and $A^+ \oplus B^+$. For $J > 0$, levels both parities occur. $C_{3v}(M)$ cannot distinguish between even and odd parity levels (because the inversion operation is not an element of the group) and should not be used.

As discussed by Babikov,[29] and Lee and Light,[30] for $^{48}O_3$, composed of identical bosons, only states for which the total wavefunction is symmetric with respect to exchange of any two O-nuclei are allowed. In the asymptotic region, the electronic wavefunction approaches the anti-symmetric $O(^3P) + O_2(^3\Sigma_g^-)$, which means that the electronic wavefunction is anti-symmetric asymptotically. In the absence of seams of intersection, the electronic wavefunction taken to be a continuous single-valued function could be determined as anti-symmetric globally.[59] However, the seams of intersection in O_3 are well-known[60] and deep in the wells, the electronic wavefunction is symmetric,[57] the character largely that of $O(^1D) + O_2(^1\Delta_g)$.[33,34] An avoided crossing along the dissociation coordinate between the two states with these characters is largely responsible for the spurious reef feature found in many PESs such as mSSB. The asymptotically anti-symmetric electronic wavefunction has been taken to dictate that high-lying allowed rovibrational states are therefore of symmetry B^+ or B^-, namely, $(-1)^{l_1+P} = -1$ in Eq. (9) (in order to make the total wavefunction symmetric as required for bosons).[29,30] This would mean that for $J = 0^+$ (even parity), only high-lying B vibrational states are allowed. (Note a typo referring to the allowed states as $J = 0^-$ appears in Lee and Light.)[30] Correspondingly, each high-lying $J = 1^+$ allowed state would be approximately a product of an A vibrational state and a rotational factor of symmetry B (due to factor of $(-1)^{K+P}$, with $K = 1$ and $P = 0$) composed of $K = +/-1$ symmetric top functions (see Table S1 of the supplementary material[44]). We note that the highest lying rovibrational wavefunctions span much of the PES making it questionable that one should fix their symmetry based on the symmetry of the electronic wavefunction near the dissociation asymptote. An avenue for future work is to construct coupled diabatic states for several electronic states of ozone which will permit a more globally consistent treatment. The adiabatic representation has been used so far (and also here), justified by the wide energy separation between states.

Noting the asymptotic antisymmetric electronic state character, Babikov reports the B vibrational states as allowed for $J = 0$ (and only reports the highest few levels).[29] Lee and Light follow the same derivation but report all of the bound levels for $J = 0$, describing the B vibrational states as allowed.[30] As discussed by Tyuterev *et al.*[26] for the states deep in the wells, it is the symmetric (A) vibrational states that are allowed for $J = 0$. Tyuterev *et al.*[26] compare their $J = 0$ B states with experimental band origins for the B states. (The low lying vibrational states are usually treated using C_{2v} symmetry and considered as localized in one well.)

To facilitate comparisons with previous studies in Table II, we report the highest $J = 0$ B-states and $J = 1$ A-states. Given that we are using a single adiabatic PES and the symmetry issues discussed above, in the supplementary material,[44] we report both the A and B type levels for both $J = 0$ and $J = 1$.[44]

The parity-adapted basis can be factorized as

$$u_{l_1;K}^{JP} = \Theta_{l_1}^{K} R_{JK}^{P}, \tag{10}$$

where

$$R_{JK}^{P} = N_K \frac{1}{\sqrt{2}} \left[|JK\rangle + (-1)^{J+K+P} |J\bar{K}\rangle \right] \tag{11}$$

is a parity-adapted rotational basis function since $E^* |JK\rangle = (-1)^{J+K} |J\bar{K}\rangle$,[61–63]

$$\sigma_{ex} R_{JK}^{P} = (-1)^{K+P} R_{JK}^{P}. \tag{12}$$

One can approximate a rovibrational wavefunction as a product of vibrational and rotational factors. The symmetry of the rotational factor can be deduced from the parity-adapted rotational basis function R_{JK}^P: it simply depends on the prefactor $(-1)^{K+P}$. This factorization explains for a given J, how the states of each symmetry are constructed by matching each vibrational state with a rotational factor expanded in terms of basis function R_{JK}^P labeled by K, as summarized in Table S1 (supplementary material).[44]

The Lanczos algorithm[64] is a common workhorse for obtaining eigenvalues of large matrices.[45,65–68] We used the RV3 code[69] by Wang and Carrington to perform our calculations, which has a parallel implementation, producing both eigenvalues (levels) and eigenvectors (wavefunctions). The rovibrational Hermitian Hamiltonian is expressed in Jacobi coordinates and is well known.[56,70]

Since the goal was to converge all of the bound states including those that span a broad range of coordinates, we did not use the Potential Optimized DVR (PODVR),[71,72] but rather used primitive sine DVR functions for the r_1 and r_0 coordinates, and a Legendre FBR for the θ coordinate (for $J = 0$) and symmetry-adapted shared-K FBR for the bend-rotation basis functions.

TABLE II. Vibrational energies (cm^{-1}) of $^{48}O_3$ states with B ($J = 0^+$) and A ($J = 1^+$) vibrational component symmetries close to dissociation (see text).

B ($J = 0^+$)			A ($J = 1^+$)		
State no.	(v_1, v_2, v_3)	$D_0 - E$	State no.	(v_1, v_2, v_3)	$D_0 - E$
102	0, 11, 1	−298.60	134		−297.16
103	1, 7, 3	−267.84	135		−257.00
104		−242.22	136		−244.66
105		−228.64	137	6, 3, 0	−234.52
106	7, 0, 1	−219.89	138	1, 11, 0	−185.49
107		−202.07	139		−175.13
108		−139.67	140		−167.25
109		−129.54	141		−151.15
110		−102.17	142		−135.72
111		−95.69	143		−120.39
112		−87.20	144		−99.82
113		−81.84	145		−96.21
114		−78.85	146		−80.27
115		−76.98	147	8, 0, 0	−74.84
116		−66.79	148		−71.02
117		−58.74	149		−54.05
118		−50.30	150		−48.58
119		−42.39	151		−39.20
120		−34.25	152		−37.70
121		−29.37	153		−28.97
122		−24.82	154		−23.97
123		−19.42	155		−23.17
124		−14.40	156		−18.23
125		−4.94	157		−11.16
			158		−8.32
			159		−4.52
			160		−1.02

For most of the reported three well calculations, 400 sine DVR points were used for r_1 and r_0 with respective ranges of [0, 14] and [1.4, 15] bohrs. An l_{max} of 150 was used for the Legendre angular FBR so the total size of the vibrational basis is 24×10^6. Tests with vibrational bases as large as 64.8×10^6 ($600 \times 600 \times 180$) and ranges of r_1 and r_0 extending out to 24 bohrs were used to check the convergence of the results. Masses of 15.994 914 619 57, 16.999 131 756 50, and 17.999 159 612 86 amu were used for ^{16}O, ^{17}O, and ^{18}O, respectively.[73] About 900 000 Lanczos iterations were needed to converge all the bound levels for the $^{48}O_3$ isotopomer. Fewer iterations were used for the lower levels to avoid excessive numbers of copies.

The A_1', A_2', and E' irreps of the $D_{3h}(M)$ group are obtained as A, B, and $(A + B)$, respectively, when Jacobi coordinates are used. Using the vibrational basis of 24×10^6 functions, the degeneracy of the $(A + B)$ pair representing the lowest E'-state is captured to better than 2×10^{-8} cm^{-1} (about the numerical tolerance employed in the Lanczos algorithm). For the lowest energy states deep in the wells, where the tunneling splitting is tiny, the A state obtained for A_1' or the B state obtained for A_2', should be degenerate with the respective A or B component obtained for the E' state. Using the basis of 24×10^6, degeneracy is obtained for the lowest A_1' and E' states to within 2×10^{-3} cm^{-1}. This is further reduced to 2×10^{-4} cm^{-1} for the larger basis of 64.8×10^6. The small splitting permits the A_1' and A_2' states to be distinguished from the two components of the E'. Near the top of the wells, tunneling splitting perturbs and splits the levels. When interpreting the smaller basis results of Grebenshchikov *et al.*,[27] Lee and Light[30] found that for the highest levels, the tunneling splittings and those due to the incomplete basis in Jacobi coordinates were of the same magnitude and adopted the convention of assigning the lowest value obtained as the A_1' or A_2' state. This was not necessary here as using the basis of 24×10^6 functions, all the states could be assigned unambiguously. For example, the numerical splitting of the two components of the E' state corresponding to the A_1' states remained small, finally reaching 0.004 cm^{-1}, 0.006 cm^{-1}, and 0.104 cm^{-1} for the last three bound states (states no. 158-160). The splitting of the A_1' states from the E' state $(A + B)$ component pairs was always much larger, beginning at 0.002 cm^{-1} for the lowest state and reaching ~0.5 cm^{-1} for the highest lying states. The results of these calculations are presented and discussed in Section III.

C. Improved relaxation (MCTDH)

MCTDH[40,41] is a time-dependent method in which each degree of freedom is associated with a small number of optimized single particle functions (SPFs) which, through their time dependence, allow an efficient description of dynamical

processes. The total wavefunction is expanded as a sum of products of single-particle functions,

$$\Psi(Q_1,\ldots,Q_f,t) = \sum_{j_1=1}^{n_1}\cdots\sum_{j_f=1}^{n_f} A_{j_1\cdots j_f}(t)\prod_{\kappa=1}^{f}\phi_{j_\kappa}^{(\kappa)}(Q_\kappa,t). \quad (13)$$

When mode combination is not used, f is the number of degrees of freedom of the system, $Q_1,\ldots,Q_f$ are the nuclear coordinates, $A_{j_1\cdots j_f}$ denote the MCTDH expansion coefficients, and $\phi_{j_\kappa}^{(\kappa)}(Q_\kappa,t)$ are the n_κ SPFs associated with degree of freedom κ. To solve the equations of motion, the SPFs are represented in a primitive DVR. Thus, the MCTDH method propagates a wavefunction in a small time-dependent, variationally optimized basis set of single-particle functions, which in turn are defined on a time-independent primitive basis set with N_κ points for the κth degree of freedom.

For the MCTDH algorithm to be efficient, the Hamiltonian operator must be written as a sum of products of single-particle operators. The KEO always has the required form when using polyspherical coordinates. The coordinates used in this study (Jacobi for the Lanczos calculations and both valence and Jacobi coordinates for MCTDH) are particular cases of polyspherical coordinates and the corresponding KEOs are sums of products (SOP) of one-dimensional operators. For the potential energy operator, which may not have the necessary product form, there exists a refitting procedure[74,75] implemented as the *potfit* algorithm, in the MCTDH package that is sufficient in 3D for obtaining the desired representation. Here *potfit* was able to represent the DJLLG PES with negligible error over the complete ranges of coordinates. In more than 3D, other tools for obtaining a SOP PES have important advantages.[76–79]

The block improved relaxation method[80,81] was used in our MCTDH computations. It enables one to use a method that was developed to solve the time-independent Schrödinger equation. The improved relaxation method is an MCSCF approach where the SPFs are optimized by relaxation (propagation in imaginary time) and the coefficient vector (A-vector) is determined by diagonalization of the Hamiltonian matrix evaluated in the set of the current SPFs. The block form of improved relaxation is an efficient way of computing several eigenstates simultaneously. Here a block of initial vectors was propagated to converge collectively to a set of eigenstates.

Two choices of coordinates were used to express the Hamiltonian in order to check the consistency of results (valence and Jacobi). Valence coordinates were used to compute some low-lying levels restricting the calculation to one well in the potential. Due to the high barrier between wells, levels deep in the well are not significantly perturbed by tunneling and in fact most reported calculations (including those by Tyuterev *et al.* up to 7900 cm^{-1}) have been done this way.[26] The one well results were obtained using valence coordinates with 256 sine DVR points for r_1 and r_2 ranging in [1.8, 12] bohrs and 128 Legendre DVR points restricted in the [1.05, 3.67] rad interval. For the highest levels, we used 30 and 25 SPFs for the r_i's and α, respectively. 10 SPFs were used for each of the r_i's and α for the lowest few levels and then progressively more were required to obtain converged results for the higher levels.

In addition, three-well calculations were performed for high-lying states, using the same ranges of Jacobi coordinates as were employed in the Lanczos calculations. The initial wavepackets were constructed with even or odd symmetry using projection operators.

III. RESULTS

For $^{48}O_3$, 125 A_2' bound states (B-vibrational component) were obtained below the $^{16}O + {}^{16}O_2$ ($v = 0$, $j = 1$) dissociation threshold in the $J = 0^+$ calculations. D_e for the DJLLG PES used in this study is 9275.12 cm^{-1}, while the $^{16}O_2$ ($v = 0$, $j = 1$) asymptotic diatomic ZPE is 794.51 cm^{-1}. (We obtain precise agreement with the value of 791.64 cm^{-1} reported by Ruedenberg *et al.* for the hypothetical forbidden $v = 0$, $j = 0$ level on the diatomic PEC.)[55] This is seven more levels than the 118 obtained by Lee and Light for the mSSB PES. Lee and Light also reported 153 A_1' states from $J = 0^+$ calculations. To obtain the states with A-vibrational component, we computed both $J = 0^+$ A_1' levels and the $J = 1^+$ levels. We obtain 160 bound states in both sets of calculations and while the lowest level for the $J = 1^+$ calculation is shifted 4.01 cm^{-1} above that of the $J = 0^+$ calculation, the spectrum above is extremely similar, with close correspondence between the $J = 0^+$ and $J = 1^+$ spectra all the way up to dissociation. Tests with larger DVR bases (up to 64.8×10^6) and extended ranges of coordinates (out to 24 bohrs) did not yield any additional bound states. However, given the three heavy masses and the fact that the last few bound states identified in this study are diffuse with increasing amplitude at long range, it is likely that one or more additional bound states would be obtained given both a large enough basis and range of coordinates. Table II lists the states of B and A vibrational component symmetry from $J = 0^+$ and $J = 1^+$, respectively, within 300 cm^{-1} of dissociation (complete lists are provided as the supplementary material)[44] from the Lanczos calculations.

To provide a sense of the accuracy of the levels, in the supplementary material,[44] we tabulate 120 conventionally reported "band centers," which correspond to $J = 0$, one-well calculations for both symmetries. These are compared with a combined best available reference data set of mostly experimental levels where available, as well as some inferred dark states and a few missing levels predicted by the spectroscopic PES of Tyuterev *et al.*[26] For the lowest states, the values of ν_1 and ν_2 (symmetric stretch and bend) are slightly smaller than experimental values, while ν_3 (asymmetric stretch) is slightly larger. The RMSE with respect to the experiment-based reference data set is 11 cm^{-1} when considering only the lowest 20 levels. Notably, the error does not worsen drastically at higher energies as the root-mean-squared-error (RMSE) only reaches 21 cm^{-1} for the lowest 100 levels and 22 cm^{-1} for all 120 levels. The 119th and 120th levels at 6539.82 and 6563.97 cm^{-1}, respectively, reach ~77% of the current best estimate of the dissociation threshold (8563.6 ± 3.5 cm^{-1})[35] and are both predicted with errors of less than 4 cm^{-1}.

The topography of the PES for the ground electronic state of ozone is unusual in that the wells are deep, well-separated, and fairly harmonic before opening up quite abruptly about 200 cm^{-1} below D_e. Lacking submerged reefs along the dissociation paths, the DJLLG PES has slight plateaus before tending to the asymptotic quadrupole-quadrupole (leading) electrostatic interaction between the O_2 and O-atom fragments. In contrast, the reefs of the mSSB PES confine the wells up to within ~80 cm^{-1} of D_e before dipping down into the vdW wells and then back up tending to a similar shape after 7 bohrs (see Figure 2 of Ref. 20).

Figure 2 shows the cumulative number of B and A vibrational states from their respective $J = 0^+$ and $J = 1^+$ calculations as a function of energy (above ZPE). A sharp upturn in the total number of states of each symmetry is observed about 200 cm^{-1} before dissociation, corresponding to the wells abruptly opening up into the plateau region.

To help appreciate the behavior in terms of densities of states, the two sets of data plotted in Figure 2 were fit to a functional form and differentiated to obtain densities of states as a function of energy. Figure 3 shows the density of states for each symmetry. It is very clear from the plot where the PES opens up as the density of states increases steeply. It is also clear that within the wells, until ~200 cm^{-1} below dissociation, the density of states is less than 0.05 states/cm^{-1} or in other words, the average separation between states of each symmetry is more than 20 cm^{-1}. Despite the sharp increase in density of states towards dissociation, it remains below one state per 4-5 cm^{-1}, which helps to explain the non-statistical nature of the dynamics.

It is interesting to compare this behavior with H_2O which has two light atoms (favoring a lower density of states), but a single deep well (41 083 cm^{-1}) that opens gradually with a Morse-like behavior.[82] In 2010, Tennyson and coworkers reported 1150 bound vibrational levels for their latest H_2O PES.[82] In contrast to ozone which is impacted

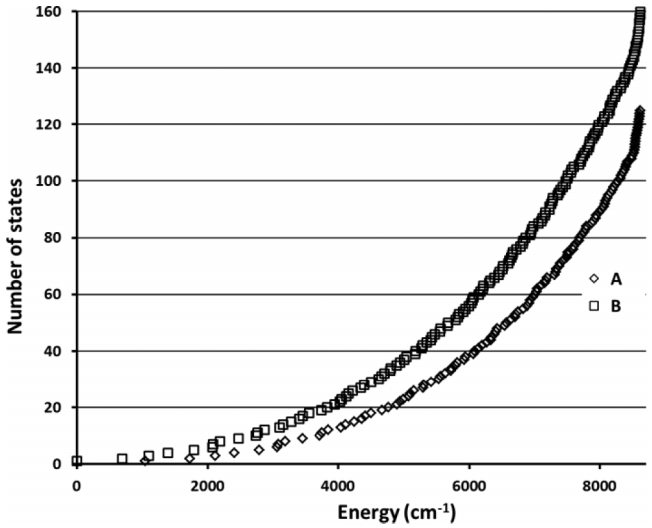

FIG. 2. Cumulative number of states with A and B vibrational component symmetry obtained in three-well calculations of $^{48}O_3$ (see text). A sharp upturn in the number of states occurs ~200 cm^{-1} below dissociation corresponding to a plateau region of the PES.

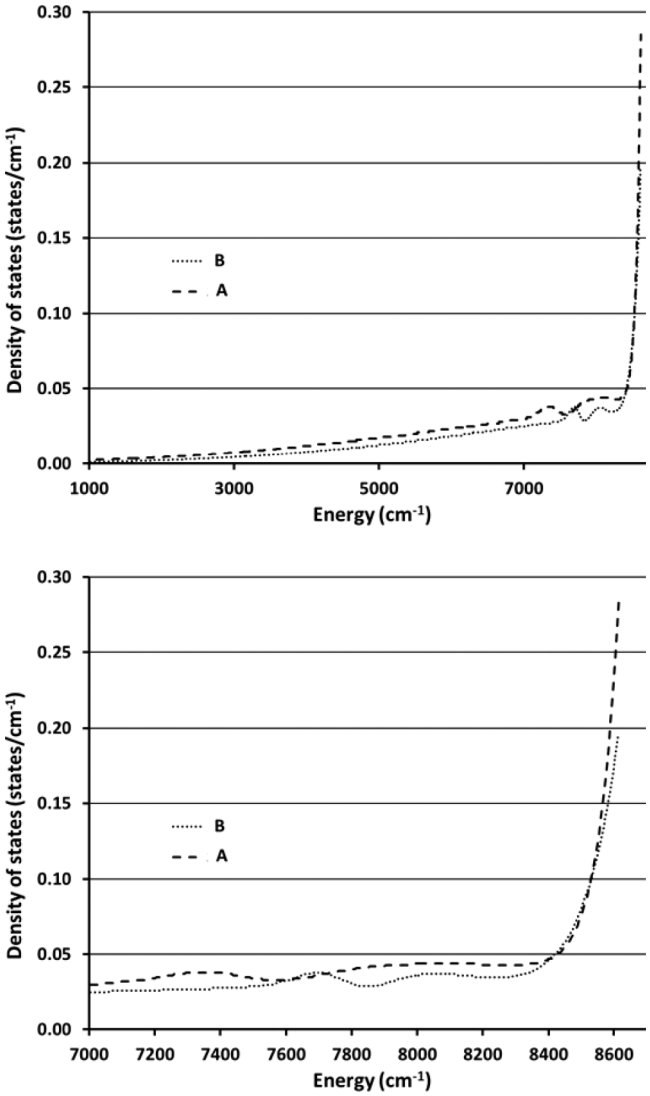

FIG. 3. (Upper) Plot of densities of bound states of B and A vibrational component symmetries as a function of energy. (Lower) Same data plotted with smaller range of energies.

by the abrupt plateau of the PES, the cumulative number of states (previously plotted by Tennyson in 1998)[83] for water smoothly increases (like the early part of Figure 2) all the way to dissociation with no sharp increase near the top. Correspondingly, the density of states for water smoothly increases to ~0.1 states/cm^{-1} near dissociation, which is similar to the combined symmetries of the all-heavy-atom O_3, except for the last few states. Lacking the abrupt transition, water has some assignable progressions very close to dissociation.

For ozone, the calculated densities of states alone are surprisingly similar for the mSSB PES. The data plotted in Figure 4 were created by similarly processing the levels reported by Lee and Light[30] and a comparable pattern including some oscillatory structure before a sharp upturn toward dissociation is observed.

The reef feature in the mSSB PES was found to disrupt the vibrational progressions and yield mainly states localized either in the main wells, or in the vdW wells, but only a few with mixed character.[27] Lacking the reef feature, no

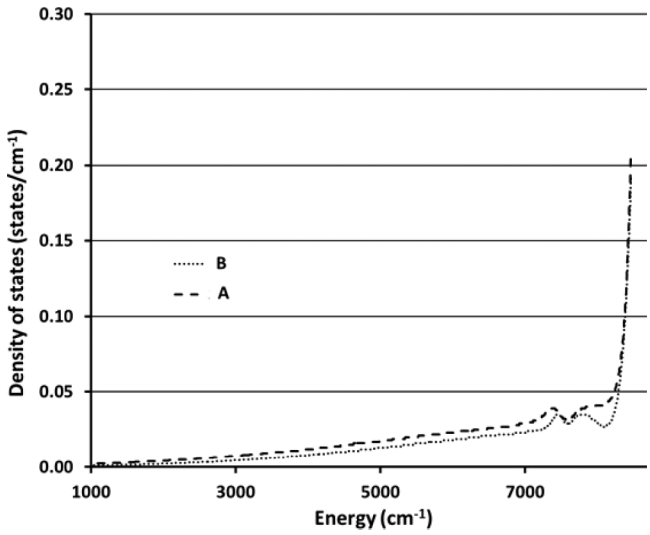

FIG. 4. Densities of states reported by Lee and Light[30] for the mSSB PES are remarkably similar to those of the DJLLG PES shown in Figure 3.

such behavior is found for the DJLLG PES. States more than 200 cm^{-1} below the dissociation energy do not have significant amplitude outside the wells. Higher in energy, progressions of states with increasing amplitude outside the main wells, extending toward dissociation along the r_0 and r_1 coordinates are observed. These high-lying states are not assignable in terms of the normal mode state labels that are useful deep in the wells. The nodal character of the parts of the wavefunctions in the wells is extremely complex, but simpler patterns of nodes are seen toward dissociation. There are a few exceptions, where some high-lying states are mostly localized in the wells (e.g., highly bend-excited states). Figure 5 shows a series of wavefunction plots for $J = 0^+$ A_2' (B-vibrational component) states entering the transition region. States near and above the plateau in the PES at approximately −200 cm^{-1} begin to show amplitude toward dissociation.

Figure 6 shows selected states near and slightly closer than 100 cm^{-1} from dissociation. In this energy region, most states have amplitude toward dissociation, but some remain localized in the wells.

Figure 7 shows all of the last 11 bound $J = 0^+ A_2'$ (B-vibrational component) states for $^{48}O_3$. All of these highest lying states have amplitudes and nodal structures along the dissociation coordinates. However, it is clear that four of them are different, being much more delocalized in the bending angle between wells.

Calculations of all the bound states were also performed for the $^{50}O_3$ ($^{16}O_2{}^{18}O$) and $^{49}O_3$ ($^{16}O_2{}^{17}O$) isotope combinations. The natural abundances of ^{16}O, ^{17}O, and ^{18}O are 0.997 57, 0.000 38, and 0.002 05, respectively.[84] Given the higher abundance and more pronounced mass difference, we focus on the $^{50}O_3$ isotopologue with complete results given in the supplementary material.[44] The dissociation threshold, $^{16}O + {}^{16}O^{18}O$ ($v = 0$, $j = 0$), is ~25 cm^{-1} lower than for $^{48}O_3$, due to the mass difference and the fact that all j-values of the $^{16}O^{18}O$ fragment are allowed. Using the same coordinate ranges and the basis with 24×10^6 vibrational functions as for $^{48}O_3$, 465 bound levels of even symmetry and 429 of odd symmetry were obtained. This compares with 430 and 395 even and odd states, respectively, reported by Lee and Light for the mSSB PES.[30] The lowest even state is the (0, 0, 0) ZPE level localized in the $^{16}O^{18}O^{16}O$ C_{2v} symmetric well. The next even state (14.3 cm^{-1} above) is a symmetric state with equal amplitude in the two asymmetric C_s $^{18}O^{16}O^{16}O$ wells. The corresponding wavefunction plots are shown in Fig. 8. The lowest odd state is the antisymmetric partner (localized in the $^{18}O^{16}O^{16}O$ wells) at the same energy (14.3 cm^{-1}). (Numerically, they differ by less than 2×10^{-8} cm^{-1}.) Since the barriers between wells are large, the low lying states

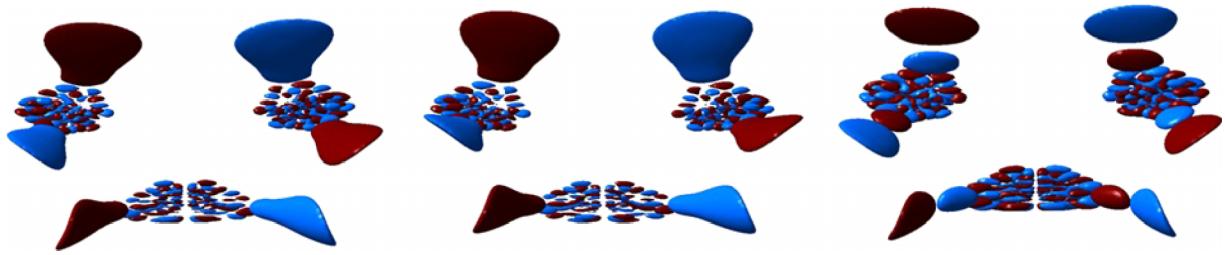

FIG. 5. Wavefunction plots for progression of $^{48}O_3$ $J = 0^+$ A_2' (B-vibrational component) states with energies of $(E - D_0) = -242.2$ cm^{-1} (left), −139.6 cm^{-1} (middle), and −129.5 cm^{-1} (right) (states 104, 108, and 109 in left side of Table II).

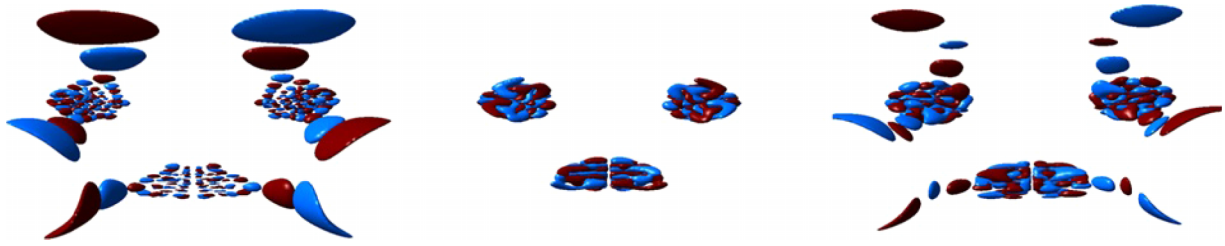

FIG. 6. Wavefunction plots for progression of $^{48}O_3$ $J = 0^+$ A_2' (B-vibrational component) states with energies of $(E - D_0) = -102.2$ cm^{-1} (left), −95.7 cm^{-1} (middle), and −81.8 cm^{-1} (right) (states 110, 111, and 113 in left side of Table II). State 111 is localized in the three wells.

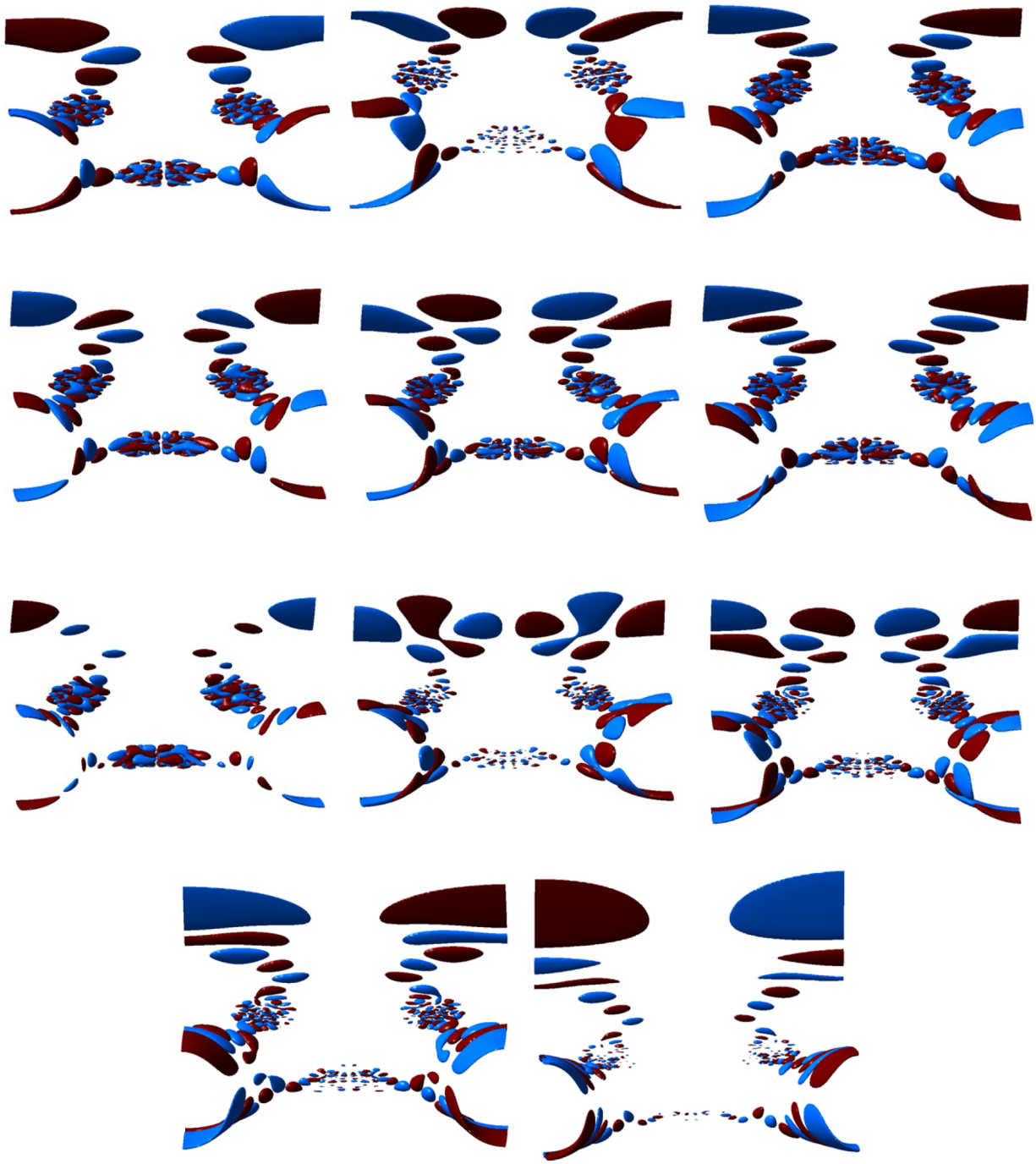

FIG. 7. Wavefunction plots for the last 11 bound $J = 0^+$ A_2' (B-vibrational component) states for $^{48}O_3$ (states 115-125 of Table II). The last state is bound by only 4.9 cm^{-1}.

localized in either the $^{16}O^{18}O^{16}O$ or $^{18}O^{16}O^{16}O$ wells are commonly considered as distinct chemical species (and can be assigned separate partition functions, etc.). The low-lying states for each isomer can be conveniently obtained in one-well calculations, by restricting the ranges of coordinates. In our global three-well calculations, the various states are only separated into even and odd (mixing together the results for states of the C_{2v} and C_s isomers).

Close to dissociation, the states tunnel between wells and are not simply assignable as separate isomers. (As an avenue for future work, to enable evaluating partition functions right up to dissociation, Ruscic suggests defining a dividing surface and integrating probability densities to assign fractions of each high-lying state to the C_{2v} and C_s isomers.)[85] Some states quite high up in energy are rather well localized in the C_{2v} or C_s wells. Figure 9 shows even states numbered 423-425 only 85.0, 84.5, and 80.9 cm^{-1} below dissociation, respectively, but clearly localized as C_{2v} and C_s isomers.

Even $^{50}O_3$ states 424 and 425, localized in the C_s wells (Figure 9), have odd counterparts (odd states 389 and 390), with tunneling splittings of just under 0.01 cm^{-1}.

Figure 10 plots the five highest lying states of even (upper panel) and odd (lower panel) symmetries. Most of the highest states have significant amplitude in all three wells, and a

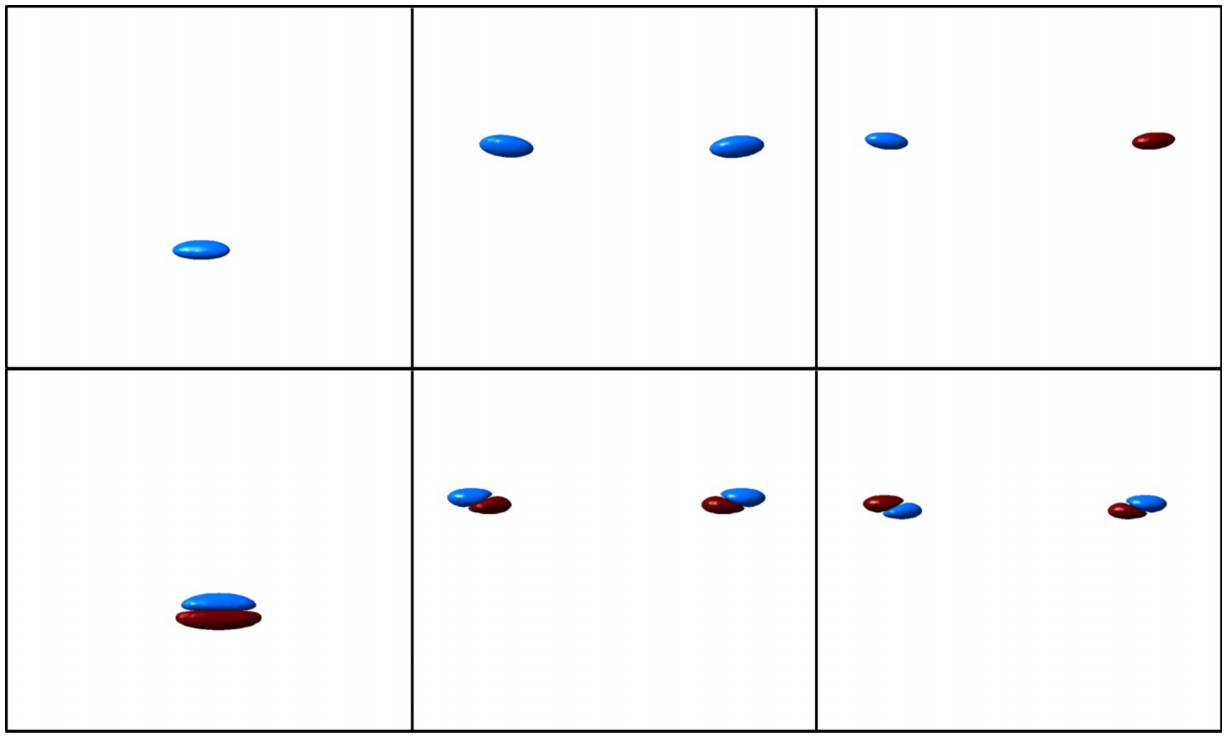

FIG. 8. (Upper left) First even $^{50}O_3$ state (0,0,0) level of C_{2v} $^{16}O^{18}O^{16}O$ isomer. (Upper middle and right) Even and odd combinations of (0,0,0) level of C_S $^{18}O^{16}O^{16}O$ isomer localized in two equivalent wells (14.3 cm^{-1} above). (Lower panel) Same as upper, but for (0,1,0) bend excited states of the two isomers.

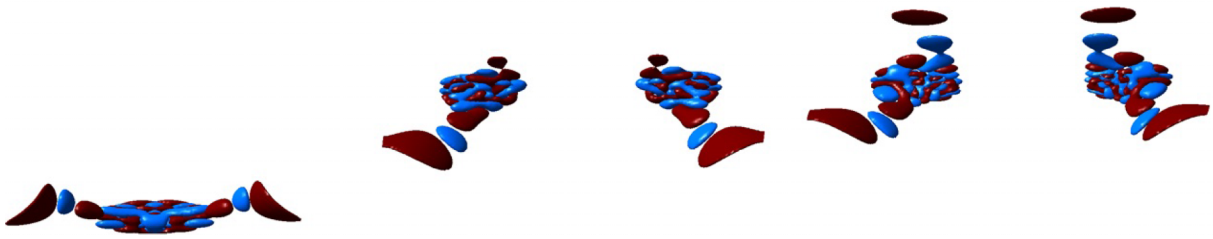

FIG. 9. Even state numbers 423-425 of $^{50}O_3$ at 85.0, 84.5, and 80.9 cm^{-1} below dissociation are clearly localized as C_{2v} and C_s isomers. Tunneling splittings with the odd counterparts of the two C_s states at right are ~0.01 cm^{-1}.

lot of amplitude and nodal patterns along the dissociation coordinates. It is notable that many of the states have more amplitude along the two paths dissociating to an ^{16}O-atom (leaving behind the more stable $^{18}O^{16}O$ diatom), than along the path to dissociating the ^{18}O-atom (leaving behind the less stable $^{16}O^{16}O$ diatom).

The complementary processes of ozone formation (step (3a)) and exchange (step (3b)) depend on the nature of near

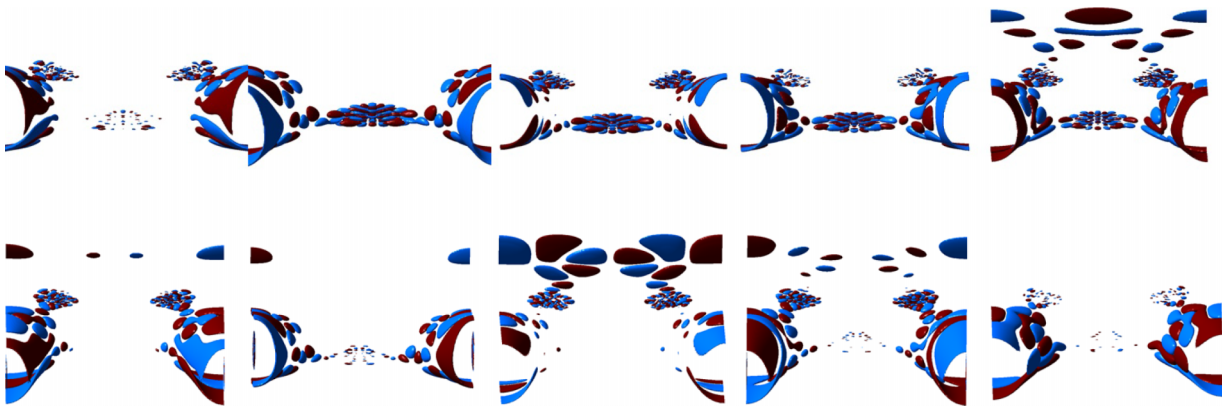

FIG. 10. (Upper) Highest five even $^{50}O_3$ states, numbered 465-461, from left to right. These even states are at energies of only −1.29, −2.06, −3.05, −4.07, and −4.91 cm^{-1} relative to the dissociation threshold. (Lower) Highest five odd $^{50}O_3$ states, numbered 429-425, from left to right. These odd states are at energies of only −1.18, −1.86, −2.20, −3.43, and −4.61 cm^{-1} relative to the dissociation threshold.

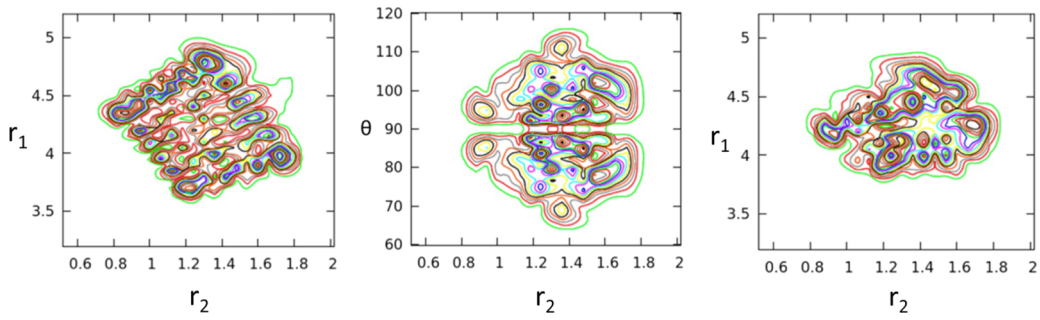

FIG. 11. (Left) One-well plot represented in valence coordinates of the (5, 0, 5) resonance state of $^{48}O_3$ computed at 35.3 cm^{-1} above the dissociation threshold using MCTDH. This resonance is short-lived (56.7 ps). (Middle and right) Two views of (unassignable) long-lived resonance (813 ps) 67.2 cm^{-1} above the dissociation threshold.

threshold resonances.[14] We have found that for the exchange reactions, the important reactive resonances are those that overlap strongly connecting the diatomic reactant and product states. The fact that many of the highest lying bound states for $^{50}O_3$ have more amplitude towards dissociation of an ^{16}O-atom supports the large kinetic isotope effect that is observed (assuming that the character of the highest lying bound progressions continues into the resonances above). Conversely, for the formation process, it is the long-lived resonances that are important, surviving long enough to undergo a stabilizing collision rather than decay into one of the exchange channels. A formula given by Miller[86] (and implemented for ozone by Grebenshchikov)[87] approximates the rate of formation simply by summing over the energies and lifetimes of resonances (the largest contributions are from low-lying, long-lived resonances).

We tested the MCTDH method to compute some of the same states and to set the stage to use MCTDH for studies of unbound resonances and also third body collisional cooling of highly excited bound states. After accurately refitting the PES, both the one-well calculations in valence coordinates and three-well calculations in Jacobi coordinates agree on average with the Lanczos results to better than 0.01 cm^{-1}.[44] Preliminary MCTDH calculations of the lowest lying resonances in $^{48}O_3$ find both short-lived resonances more delocalized along the dissociation coordinates (likely relevant to the exchange processes) and remarkably localized and long-lived resonances (more relevant to the formation process). Some examples are plotted in Fig. 11. These states and dynamics will be the subject of future work.

IV. CONCLUSIONS

We report all of the bound states for three isotopic combinations of ozone ($^{48}O_3$, $^{16}O_2{}^{18}O$, $^{16}O_2{}^{17}O$) for $J = 0$ and $J = 1$, using the new DJLLG PES with a focus on the character and density of highly excited states and discuss their impact on the ozone isotopic anomaly. The DJLLG PES differs qualitatively from previous PESs such as the mSSB PES, lacking a spurious reef feature in the asymptotic region. For $^{48}O_3$, 125 bound levels of B (odd) vibrational component symmetry and 160 of A (even) vibrational component symmetry were determined. The density of states as a function of energy has a dramatic upturn ~200 cm^{-1} below dissociation due to the onset of a plateau region in the PES of ozone. The previous mSSB PES with spurious reef features has a remarkably similar density of states, but the highest states of the mSSB PES separate into well-states and vdW states (localized in the main or vdW wells respectively), whereas the states for the DJLLG PES follow unbroken progressions with significant amplitude towards dissociation. These calculations and analysis of the character of high-lying states leading into the resonances sets the stage for future work exploring the nature of the resonances contributing to the competing exchange and formation processes.

ACKNOWLEDGMENTS

This work was supported by the US National Science Foundation (No. CHE-1300945 to R.D.), and US Department of Energy (No. DE-FG02-05ER15694 to H.G.) and NSERC of Canada. Z.S. is supported through the National Basic Research Program of China (Grant No. 2013CB922200), the National Natural Science Foundation of China (Grant Nos. 21222308, 21103187, and 21133006), the Chinese Academy of Sciences, and the Key Research Program of the Chinese Academy of Sciences. S.N. thanks H.-D. Meyer for useful discussions about computing resonances using MCTDH.

[1]Y. L. Yung, A. Y. Lee, F. W. Irion, W. B. DeMore, and J. Wen, J. Geophys. Res. **102**, 10857, doi:10.1029/97JD00528 (1997).
[2]A. A. Wiegel, A. S. Cole, K. J. Hoag, E. L. Atlas, S. M. Schauffer, and K. A. Boering, Proc. Natl. Acad. Sci. U. S. A. **110**, 17685 (2013).
[3]J. Kaiser, T. Rockmann, and C. Brenninkmeijer, J. Geophys. Res. **109**, D03305 (2004).
[4]R. Criegee, Angew. Chem., Int. Ed. Engl. **14**, 745 (1975).
[5]O. Welz, J. D. Savee, D. L. Osborn, S. S. Vasu, C. J. Percival, D. E. Shallcross, and C. A. Taatjes, Science **335**, 204 (2012).
[6]Y.-T. Su, Y.-H. Huang, H. A. Witek, and Y.-P. Lee, Science **340**, 174 (2013).
[7]C. A. Taatjes, O. Welz, A. J. Eskola, J. D. Savee, A. M. Scheer, D. E. Shallcross, B. Rotavera, E. P. F. Lee, J. M. Dyke, D. K. W. Mok, D. L. Osborn, and C. J. Percival, Science **340**, 177 (2013).
[8]R. Dawes, B. Jiang, and H. Guo, J. Am. Chem. Soc. **137**, 50 (2015).
[9]S. Chapman, Mem. R. Meteorol. Soc. **3**, 103 (1930).
[10]M. H. Thiemens and J. E. Heidenreich, Science **219**, 1073 (1983).
[11]K. Mauersberger, Geophys. Res. Lett. **14**, 80, doi:10.1029/GL014i001p00080 (1987).
[12]K. Mauersberger, B. Erbacher, D. Krankowsky, J. Günther, and R. Nickel, Science **283**, 370 (1999).
[13]K. Mauersberger, P. Lämmerzahl, and D. Krankowsky, Geophys. Res. Lett. **28**, 3155, doi:10.1029/2001GL013439 (2001).

[14]Z. Sun, X. Lin, D. Yu, S. Ndengue, R. Dawes, B. Zhao, and H. Guo, "Resonance origin of kinetic isotope effects in $O + O_2$ exchange reactions and implications in non-mass-dependent fractionation of O_3" (unpublished).
[15]V. Haverd, G. C. Toon, and D. W. T. Griffith, Geophys. Res. Lett. **32**, L22808, doi:10.1029/2005GL024049 (2005).
[16]M. C. Liang, F. W. Irion, J. D. Weibel, G. A. Blake, C. E. Miller, and Y. L. Yung, J. Geophys. Res. **111**, D02302, doi:10.1029/2005jd006342 (2006).
[17]D. Krankowsky, P. Lammerzahl, K. Mauersberger, C. Janssen, B. Tuzson, and T. Rockmann, J. Geophys. Res. **112**, D08301, doi:10.1029/2006jd007855 (2007).
[18]S. A. Ndengue, S. Madronich, F. Gatti, H. D. Meyer, O. Motapon, and R. Jost, J. Geophys. Res.: Atmos. **119**, 4286, doi:10.1002/2013jd020033 (2014).
[19]R. Dawes, P. Lolur, J. Ma, and H. Guo, J. Chem. Phys. **135**, 081102 (2011).
[20]R. Dawes, P. Lolur, A. Li, B. Jiang, and H. Guo, J. Chem. Phys. **139**, 201103 (2013).
[21]Y. Li, Z. Sun, B. Jiang, D. Xie, R. Dawes, and H. Guo, J. Chem. Phys. **141**, 081102 (2014).
[22]T. R. Rao, G. Guillon, S. Mahapatra, and P. Honvault, J. Chem. Phys. **142**, 174311 (2015).
[23]R. Siebert, R. Schinke, and M. Bitterova, Phys. Chem. Chem. Phys. **3**, 1795 (2001).
[24]R. Siebert, P. Fleurat-Leussard, R. Schinke, M. Bitterova, and S. C. J. Farantos, J. Chem. Phys. **116**, 9749 (2002).
[25]M. Ayouz and D. Babikov, J. Chem. Phys. **138**, 164311 (2013).
[26]V. G. Tyuterev, R. V. Kochanov, S. A. Tashkun, F. Holka, and P. G. Szalay, J. Chem. Phys. **139**, 134307 (2013).
[27]S. Y. Grebenshchikov, R. Schinke, P. Fleurat-Leussard, and M. Joyeux, J. Chem. Phys. **119**, 6512 (2003).
[28]D. Babikov, B. K. Kendrick, R. B. Walker, R. T Pack, P. Fleurat-Lesard, and R. Schinke, J. Chem. Phys. **118**, 6298 (2003).
[29]D. Babikov, J. Chem. Phys. **119**, 6554 (2003).
[30]H.-S. Lee and J. C. Light, J. Chem. Phys. **120**, 5859 (2004).
[31]D. Babikov, personal communication (2015).
[32]M. V. Ivanov and D. Babikov, J. Chem. Phys. **134**, 174308 (2011).
[33]A. Kalemos and A. Mavridis, J. Chem. Phys. **129**, 054312 (2008).
[34]E. Miliordos and S. S. Xantheas, J. Am. Chem. Soc. **136**, 2808 (2014).
[35]B. Ruscic, Active Thermochemical Tables (ATcT) values based on version 1.112 of the Thermochemical Network, 2013, available at ATcT.anl.gov.
[36]E. Starikova, A. Barbe, M.-R. De Backer, D. Mondelain, S. Kassi, A. Campargue, and V. G. Tyuterev, Proc. SPIE **9680**, 96800L (2015).
[37]A. Campargue, S. Kassi, D. Mondelain, A. Barbe, E. Starikova, M.-R. De Backer, and V. G. Tyuterev, J. Quant. Spectrosc. Radiat. Transfer **152**, 84 (2015).
[38]Z. Sun, D. Yu, W. Xie, J. Hou, R. Dawes, and H. Guo, J. Chem. Phys. **142**, 174312 (2015).
[39]W. Xie, L. Liu, Z. Sun, H. Guo, and R. Dawes, J. Chem. Phys. **142**, 064308 (2015).
[40]*Multidimensional Quantum Dynamics: MCTDH Theory Applications*, edited by H. D. Meyer, F. Gatti, and G. A. Worth (Wiley-VCH, Weinheim, 2009).
[41]M. H. Beck, A. Jackle, G. A. Worth, and H. D. Meyer, Phys. Rep. **324**, 1 (2000).
[42]S. A. Ndengue, R. Dawes, F. Gatti, and H.-D. Meyer, J. Phys. Chem. A **119**, 12043 (2015).
[43]S. A. Ndengue, R. Dawes, and F. Gatti, J. Phys. Chem. A **119**, 7712 (2015).
[44]See supplementary material at http://dx.doi.org/10.1063/1.4941559 for details of the permutation symmetry of the parity-adapted rotational functions as well as extensive tables of the bound states of each symmetry and isotopic combination.
[45]T. Shiozaki, G. Knizia, and H.-J. Werner, J. Chem. Phys. **134**, 034113 (2011).
[46]T. Shiozaki and H.-J. Werner, Mol. Phys. **111**, 607 (2013).
[47]H. J. Werner, P. J. Knowles, G. Knizia *et al.*, MOLPRO, version 2012.1, a package of *ab initio* programs, 2012, see http://www.molpro.net.
[48]R. Dawes, D. L. Thompson, A. F. Wagner, and M. Minkoff, J. Chem. Phys. **128**, 084107 (2008).
[49]J. P. Camden, R. Dawes, and D. L. Thompson, J. Phys. Chem. A **113**, 4626 (2009).
[50]R. Dawes, A. F. Wagner, and D. L. Thompson, J. Phys. Chem. A **113**, 4709 (2009).
[51]R. Dawes, X. G. Wang, A. W. Jasper, and T. Carrington, Jr., J. Chem. Phys. **133**, 134304 (2010).
[52]M. Majumder, S. Ndengue, and R. Dawes, Mol. Phys. **114**, 1 (2015).
[53]M. Lepers, B. Bussery-Honvault, and O. Dulieu, J. Chem. Phys. **137**, 234305 (2012).
[54]B. Bussery-Honvault, personal communication (2014).
[55]L. Bytautas, N. Matsunaga, and K. Ruedenberg, J. Chem. Phys. **132**, 074307 (2010).
[56]J. Tennyson, Comput. Phys. Rep. **4**, 1 (1986).
[57]P. R. Bunker and P. Jensen, *Molecular Symmetry and Spectroscopy* (NRC Research Press, Ottawa, 1998), Vol. 2.
[58]J. M. Flaud and R. Bacis, Spectrochim. Acta, Part A **54**, 3 (1998).
[59]C. A. Mead and D. G. Truhlar, J. Chem. Phys. **70**, 2284 (1979).
[60]G. J. Atchity and K. Ruedenberg, Theor. Chem. Acc. **96**, 176 (1997).
[61]R. Jaquet and T. Carrington, J. Phys. Chem. A **117**, 9493 (2013).
[62]X.-G. Wang and T. Carrington, Jr., J. Chem. Phys. **118**, 6946 (2003).
[63]X.-G. Wang and T. Carrington, Jr., J. Chem. Phys. **121**, 2937 (2004).
[64]C. Lanczos, J. Res. Natl. Bur. Stand. **45**, 255 (1950).
[65]P. Sarkar, N. Poulin, and T. Carrington, Jr., J. Chem. Phys. **110**, 10269 (1999).
[66]M. J. Bramley and T. Carrington, Jr., J. Chem. Phys. **99**, 8519–8541 (1993).
[67]M. J. Bramley, J. W. Tromp, T. Carrington, Jr., and G. C. Corey, J. Chem. Phys. **100**, 6175 (1994).
[68]H. Guo, Rev. Comput. Chem. **25**, 285 (2007).
[69]X. G. Wang and T. Carrington, RV3: A package of programs to compute rovibrational levels and wavefunctions of triatomic molecules (unpublished).
[70]X.-G. Wang and T. Carrington, Jr., Mol. Phys. **110**, 825 (2012).
[71]J. Echave and D. C. Clary, Chem. Phys. Lett. **190**, 225 (1992).
[72]H. Wei and T. Carrington, Jr., J. Chem. Phys. **97**, 3029 (1992).
[73]A. H. Wapstra, F. G. Kondev, M. Maccormick, X. Xu, and B. Pfeiffer, Chin. Phys. C **36**, 1287 (2012).
[74]A. Jackle and H. D. Meyer, J. Chem. Phys. **104**, 7974 (1996).
[75]A. Jackle and H. D. Meyer, J. Chem. Phys. **109**, 3772 (1998).
[76]S. Manzhos and T. Carrington, Jr., J. Chem. Phys. **129**, 224104 (2008).
[77]S. Manzhos and T. Carrington, Jr., J. Chem. Phys. **127**, 014103 (2007).
[78]S. Manzhos and T. Carrington, Jr., J. Chem. Phys. **125**, 194105 (2006).
[79]G. Avila and T. Carrington, Jr., J. Chem. Phys. **143**, 044106 (2015).
[80]H.-D. Meyer and G. A. Worth, Theor. Chem. Acc. **109**, 251 (2003).
[81]H.-D. Meyer, F. Le Quéré, C. Léonard, and F. Gatti, Chem. Phys. **329**, 179 (2006).
[82]A. G. Csaszar, E. Mátyus, T. Szidarovszky, L. Lodi, N. F. Zobov, S. V. Shirin, O. L. Polyansky, and J. Tennyson, J. Quant. Spectrosc. Radiat. Transfer **111**, 1043 (2010).
[83]H. Y. Mussa and J. Tennyson, J. Chem. Phys. **109**, 10885 (1998).
[84]M. Berglund and M. E. Wieser, Pure Appl. Chem. **83**, 397 (2011).
[85]B. Ruscic, personal communication (2014).
[86]T. C. Germann and W. H. Miller, J. Phys. Chem. A **101**, 6358 (1997).
[87]S. Y. Grebenshchikov, Few-Body Syst. **45**, 241 (2009).